SSRG International Journal of Electronics and Communication Engineering
ISSN: 2348-8549/ https://doi.org/10.14445/23488549/IJECE-V12I9P103

Volume 12 Issue 9, 32-45, September 2025

Original Article

Remote Sensing-Based Land Use and Land Cover Classification Using Deep Learning with Tuna Swarm Optimisation for Hyperparameter Tuning Process

G. S. Sravanthi[1], Arulselvi Gnanasekaran[2], G. S. Ramesh[3]

[1,2]*Department of CSE, Annamalai University, Annamalai Nagar, Chidambaram, Tamil Nadu, India.*
[3]*Department of CSE, Telangana Tribal Welfare Residential Degree College, Nagarkurnool, Macharam (Village), Jadcherla (Mandal), Mahabubnagar (Dist), Telangana, India.*

[1]*Corresponding Author : sravanthikumari22@gmail.com*

Received: 03 July 2025 Revised: 05 August 2025 Accepted: 04 September 2025 Published: 29 September 2025

Abstract *- Land Use and Land Cover (LULC) are key indicators of global environmental change. As a result, the extensive effort was dedicated to creating larger-scale products of LULC from Remote Sensing (RS) data, allowing the technical group to utilize these products for a wide array of downstream applications. This phenomenon causes widespread anxiety about natural resources. Therefore, observing LULC changes was significant for natural resource management and evaluating the effects of environmental change. Machine Learning (ML) has recently gained significance for fast and accurate LULC mapping using RS data, driven by the growing requirement for ecological, environmental, and resource management. It is crucial to compute the performance of diverse ML models for reliable LULC mapping. This study proposes a novel Remote Sensing-Based Land Use and Land Cover Classification Using Deep Learning with Tuna Swarm Optimisation (RSLULCC-DLTSO) methodology. The RSLULCC-DLTSO methodology aims to advance intelligent and automated LULC classification systems that assist in sustainable land management and environmental decision-making. In the pre-processing stage, the RSLULCC-DLTSO technique utilizes a Wiener Filtering (WF) model to eliminate noise and enhance the quality of satellite images. Furthermore, the DenseNet-121-based feature extraction captures hierarchical spatial patterns and textures from RSI. A Variational Autoencoder (VAE) model is also used for LULC classification. Finally, the Tuna Swarm Optimisation (TSO) model optimally adjusts the hyperparameter values of the VAE technique, resulting in improved classification performance. A wide range of simulation analyses of the RSLULCC-DLTSO approach is implemented under the EuroSat dataset. The comparative study of the RSLULCC-DLTSO approach illustrated a superior accuracy value of 98.57% compared to existing models.*

Keywords *- Land Use and Land Cover, Deep Learning, Tuna Swarm Optimisation, Remote Sensing, Image Pre-processing.*

1. Introduction

LULC control is a dynamic process that is constantly evolving and changing due to various environmental and human impacts [1]. The continuous advancement of technology has led to significant transformations in the environment. Urban areas have diverse land uses, and these uses are evolving and changing rapidly worldwide. Consequently, recurrent change recognition analysis is significant for recognizing the negative and positive variations in land cover [2]. RS images are used in change detection models to detect land cover variations without the requirement for field investigation. Change detection and LULC classifications are related to the area of Geographic Information Systems (GIS) and RS [3]. It acquires the Earth's surface data, whereas the GIS process visualizes and analyses spatial data. Using RS imagery, LULC classification encompasses various types of land cover, including urban areas, agricultural land, and forests [4]. This serves as a primary data source for analyzing variance, intended to explore and identify changes. By comparing LULC maps from diverse periods, researchers can detect changes like urban growth, intensified agriculture, and deforestation [5]. These perceptions are vital for resource management, urban planning, and environmental monitoring, giving a clear understanding of how natural processes and human actions change the landscape [6].

Therefore, effective LULC classification is crucial for trustworthy change recognition. Conventional approaches, such as manual digitization of satellite imagery and visual interpretation, often lead to human error [7]. ML models can resolve classification problems, predict RS images, and

detect anomalies. Generally, ML models are employed to classify images using the most suitable classifiers, such as K-Nearest Neighbour (KNN), Artificial Neural Network (ANN), Support Vector Machine (SVM), Markov Chain model, and others [8]. With the increasing amount of Earth data and the development of ML models, innovative modelling is introduced, which can manage vast amounts of data and improve predictive analysis of temporal and spatial features through Deep Learning (DL) [9]. The DL method has surpassed conventional methods in removing spatial multi-level extracted features from RS images, enabling better classification and image processing [10]. The aim is to incorporate DL models to produce reliable results for detecting LULC changes. Accurate LULC is significant for monitoring environmental variances, urban expansion, and resource administration. Conventional methods mostly lack scalability and precision, particularly in intrinsic terrains. The integration of DL with remote sensing presents an ideal solution for capturing detailed spatial patterns. Efficient tuning additionally improves the accuracy and adaptability across diverse landscapes.

This study proposes a novel Remote Sensing-Based Land Use and Land Cover Classification Using Deep Learning with Tuna Swarm Optimisation (RSLULCC-DLTSO) methodology. The RSLULCC-DLTSO methodology aims to advance intelligent and automated LULC classification systems that assist in sustainable land management and environmental decision-making. In the pre-processing stage, the RSLULCC-DLTSO technique utilizes a Wiener Filtering (WF) model to eliminate noise and enhance the quality of satellite images. Furthermore, the DenseNet-121-based feature extraction captures hierarchical spatial patterns and textures from RSI. A Variational Auto Encoder (VAE) model is also utilized for the LULC classification process. Finally, the Tuna Swarm Optimisation (TSO) model optimally adjusts the hyperparameter values of the VAE technique, resulting in improved classification performance. A wide range of simulation analyses of the RSLULCC-DLTSO approach is implemented under the EuroSat dataset. The significant contribution of the RSLULCC-DLTSO approach is listed below.

- The RSLULCC-DLTSO model effectively utilizes WF to mitigate noise in input data. Enhancing the image clarity contributes to improved feature extraction and classification accuracy. This step confirms cleaner input for DL components, strengthening the method's overall performance.
- The RSLULCC-DLTSO approach utilizes the DenseNet-121 technique to extract deep, high-dimensional features from input data, thereby enhancing its representational capacity. Its dense connectivity facilitates feature reuse and mitigates the risk of vanishing gradients, thereby improving the capacity to comprehend intrinsic spatial patterns crucial for accurate LULC classification.
- The RSLULCC-DLTSO methodology implements the VAE model for effective and probabilistic classification by learning latent representations of input data. It models uncertainty in predictions, which enhances the model's robustness in intrinsic scenarios. This integration assists in more accurate and reliable detection of LULC changes.
- The RSLULCC-DLTSO method utilizes the TSO model to fine-tune the model parameters, ensuring optimal convergence and performance. This bio-inspired algorithm improves the model's adaptability to varying data distributions. It enhances classification accuracy and computational efficiency in LULC detection.
- The novelty of the RSLULCC-DLTSO model lies in its integration of WF, DenseNet-121, VAE, and TSO into a single, cohesive framework. This integration utilizes the merits of each method to address challenges in LULC change detection more effectively. The framework offers enhanced accuracy and adaptability across diverse environments by incorporating noise reduction, deep feature extraction, probabilistic classification, and optimization.

2. Related Works

In [11], the U-Net structure is improved by incorporating SK ResNeXt as the encoder for the LCC challenge, utilizing MSI. SK-ResNeXt presents the size of the adaptive kernel and cardinality, enabling the U-Net to take multiple-scale aspects and fine-tune more effectually to change spatial resolution. Rubab et al. [12] projected an innovative network-level fusion deep structure depending on SIB-Net and 16-tiny ViT. At the primary level, data augmentation is employed to address concerns about data imbalance. A self-attention bottleneck-based Inception CNN model called SIB-Net is projected to a higher level. The blocks are designed to utilize the inception framework; bottleneck blocks are formed in every module. The 16-tiny Vision Transformer (ViT) is applied to RS images, integrated with SIBNet via network-level fusion, and trained using Bayesian-optimised hyperparameters. Majidi et al. [13] developed a combination of dense point clouds and multiple-spectral imaging, utilizing a dual-stream deep convolution method that incorporates elevation data and vegetation into spectral data. Depending on the modality framework, a dual-stream Deep Neural Network (DNN), as specified in the Deeplabv3+ framework, is executed to fuse either modality feature. Moreover, the Xception method is deliberated as a feature extractor and backbone. In [14], remotely sensed data are employed to formulate an advanced DL method for wide-ranging Earth observation. The foundation of this method contains the advancement of the 3-layered CCM-CNN method. Initially, images are extracted before being fed into the 3-layered CCM-CNN framework. In [15], an innovative label refinement method is proposed, transforming noisy original LR labels into refined HR labels utilizing dual stages of noise

filtering. Primarily, the method selects moderately confident labels from the LR labels using spectral indices from the HR images, and then optimizes them over a Markov Random Field structure. Afterwards, a shallow classifier like RF is trained to utilize the selected pixels to supplement formerly unselected labels and refine lower-confidence labels with novel and higher-confidence labels. In [16], LULC change prediction and classification utilizing DCSNN and EESNN are presented. Additionally, the images are pre-processed using the FDCT-WRP model. For classification, the DCSNN is utilized in the post-classification method.

In [17], an innovative SSM for LC change detection (LCCDMamba) is introduced to employ Siam-VMamba as a backbone. The MISF method is designed to integrate change information across different temporal periods. The presented model incorporates MSFA and uses strip convolution to integrate multi-scale local change data of residuals with SS2D (RSS) and bi-temporal land cover features. It utilizes a residual framework with SS2D to acquire global variances of bi-temporal land cover aspects. DTMS also intends to use two token modelling methods. Gowri et al. [18] presented a novel Convolutional Neural Network (CNN) technique, namely Hypergraph CNN (HGCNN), for classification. It extracts residual features and integrates them into hyper-edges for enhanced classification accuracy. Alqadhi et al. [19] utilized advanced models and DNNs to quantify land cover changes, urban expansion, and ecological impacts. Bhatti et al. [20] presented a deep network-level fusion approach that integrates a stacked residual self-attention CNN (SRAN3) with a lightweight ViT, utilizing four encoders to improve performance while mitigating computational costs. The models are integrated using depth concatenation, and hyperparameters are optimized via the Bayesian Optimization (BO) model for enhanced learning and classification accuracy. Rega and Sivakumar [21] proposed the Automated RS Image Classification by employing the Horse Herd Optimisation with Deep Transfer Learning (ARSIC-HHODTL) technique. It utilizes Bilateral Filtering (BF) for noise removal, EfficientNet-B7 for extraction, and LSTM for classification, with the HHO model for improving the model's performance. Vaghela et al. [22] utilized the YOLO V8 approach to classify agricultural lands from RS images, computing diverse YOLO V8 versions and analyzing the impact of hyperparameters. Mangkhaseum et al. [23] developed flood susceptibility maps using DL techniques, namely ANN, LSTM, DNN and open-source datasets. Jayanth et al. [24] improved CNNs using metaheuristic approaches, specifically Artificial Bee Colony (ABC) and Grey Wolf Optimization (GWO), to detect and classify RS data. Fan et al. [25] introduced a framework that integrates denoising diffusion probabilistic models and ViT for an improved LULC segmentation approach (DDPM-SegFormer). It generates refined semantic features and models global image context.

Onojeghuo et al. [26] developed a DL methodology to analyze wetland dynamics in the Niger Delta utilizing multi-temporal, multi-sensor satellite data. Lu et al. [27] introduced a CNN-BiGRU model improved with a novel GCBA attention mechanism for estimation utilizing multi-variable RS data. Shailaja et al. [28] developed a Land Cover Classification Network (LCC-Net) for accurate classification by utilizing the Enhanced Super-Resolution Generative Adversarial Network (ESRGAN) technique for image enhancement, and Swin transformer CNN (ST-CNN) with Adaptive Moment Estimation (AME) optimizer for classification. Sawant and Ghosh [29] trained five DL methods for accurate pixel-wise classification. Maashi et al. [30] evaluated the impacts of LULC changes on agriculture using Landsat satellite imagery and the Random Forest (RF) model. Chroni et al. [31] integrated multispectral imagery and airborne Light Detection and Ranging (LiDAR) data by utilizing a CNN-based U-Net semantic segmentation model. Tadesse et al. [32] proposed a data-centric framework by utilizing a teacher–student model for generating accurate local land-cover maps in Africa by employing high-resolution (0.331 m/m/pixel) and low-resolution (10 m/m/pixel) satellite images. Jhonnerie et al. [33] incorporated Microsoft Copilot for code generation and Google Earth Engine (GEE) for Sentinel-2 image processing and classification using the RF approach. Tang et al. [34] introduced a DL-based framework by utilizing remote sensing images by incorporating online and offline data augmentation, the EfficientNet_Large model for extraction, and an SVM classifier for classification. Baek, Lee, and Jung [35] proposed a Separated-Input-Based U-Net (SiU-Net) technique that processes Red-Green-Blue (RGB) and Near-Infrared (NIR) bands separately. Ewunetu and Abebe [36] analyzed LULC changes in the Upper Tekeze Basin using Google Earth Engine (GEE) and the RF classifier. Arain et al. [37] improved LCLU classification of hyperspectral and RGB images utilizing DL models, comprising 2D and 3D CNN, Long Short-Term Memory (LSTM), Gated Recurrent Units (GRU), bidirectional LSTM, and pre-trained CNNs such as VGG16, VGG19, ResNet50, ResNet50 V2, and MobileNet.

Despite various advancements in LULC classification by utilizing DL and hybrid models, diverse limitations still exist. Several methods face difficulty with imbalanced and limited training data, affecting model generalization and robustness. High computational costs and intrinsic architectures restrict scalability and real-time applications, specifically in resource-constrained settings. Furthermore, the accuracy is mitigated by spectral confusion and noise in multispectral and hyperspectral data. Most models concentrate on single-modality data or lack effective fusion strategies for multi-source inputs like LiDAR and MSI. The research gap is in developing lightweight, scalable frameworks that effectually handle multi-modal data, address data imbalance, and optimize hyperparameters dynamically while maintaining

high accuracy and generalization across diverse environments.

3. Methodology

This paper proposes the RSLULCC-DLTSO methodology. The methodology aims to advance intelligent and automated LULC classification systems that assist in sustainable land management and environmental decision-making. Figure 1 illustrates the overall flow of the RSLULCC-DLTSO approach.

3.1. Image Pre-processing: WF Model

In the pre-processing stage, the RSLULCC-DLTSO technique utilizes WF to extract noise and to improve the quality of satellite images [38]. This technique is chosen for its efficiency in mitigating noise while conserving crucial features in the image. Unlike other noise reduction models, such as Gaussian smoothing or median filtering, WF adapts to local signal characteristics, enabling more precise noise suppression without compromising fine details.

The model also performs by computing the original signal based on statistical properties, resulting in a clearer image for subsequent analysis. This adaptability makes WF suitable for intrinsic and noisy datasets, ensuring that the input data retains the maximum information for downstream tasks. Moreover, its computational efficiency and capability to handle diverse types of noise make it a superior choice to conventional methods. Hence, the model highlights a balance in noise reduction and feature preservation, which is crucial for effective LULC change detection. Figure 2 depicts the architecture of the WF method.

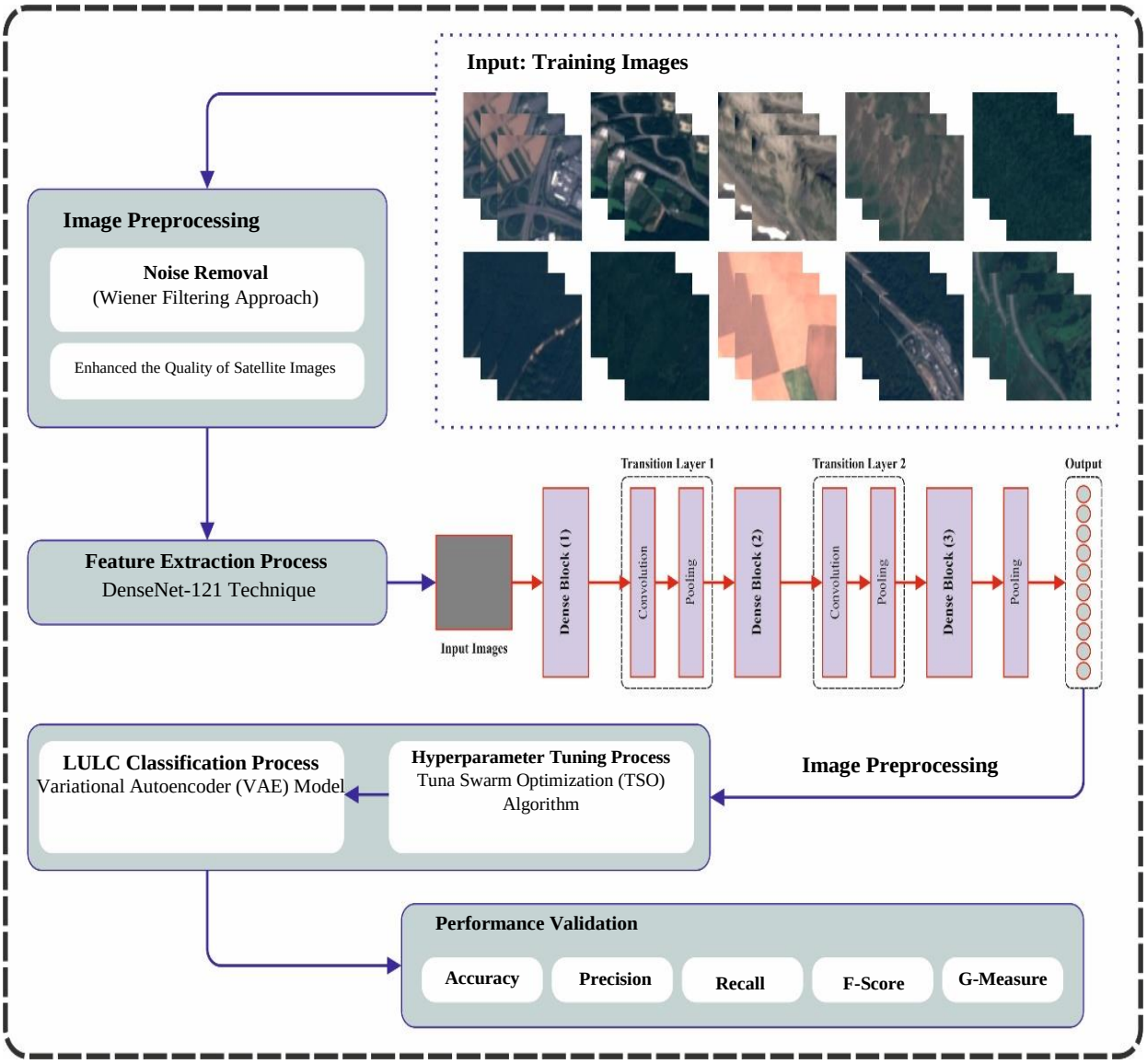

Fig. 1 Overall flow of the RSLULCC-DLTSO model

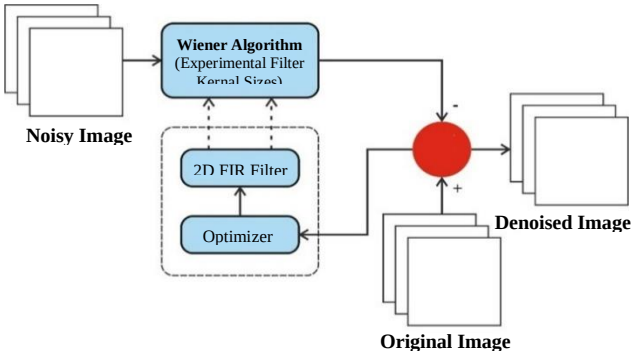

Fig. 2 Structure of the WF model

WF is an adaptive noise reduction model employed in image pre-processing to classify LULC in RS. It efficiently eliminates Gaussian noise while upholding fine and edge details, improving the quality of satellite images. By assessing the local variance, WF enhances the extraction of features for superior classification accuracy. It helps improve spatial and spectral information, making land cover features more accurate and reliable. This pre-processing stage considerably increases the achievement of DL and ML techniques in LULC classification.

3.2. Feature Extraction

Furthermore, the DenseNet-121-based feature extraction captures hierarchical spatial patterns and textures from RSI [39]. This model is selected for its dense DL architecture, where each layer connects to all others. The model also emphasizes improved propagation and reuse, significantly mitigating the risk of vanishing gradients and improving model convergence.

Unlike conventional CNNs, DenseNet-121 facilitates learning richer, more diverse features through dense connections, making it highly effective for intrinsic tasks such as LULC change detection. Its capability to capture fine-grained spatial patterns while reducing the number of parameters enables high performance without overfitting. Moreover, the model's superior accuracy and computational efficiency make it an ideal choice for large-scale image analysis, giving both high feature extraction capability and robust generalization across diverse datasets. Figure 3 specifies the structure of the DenseNet-121 approach.

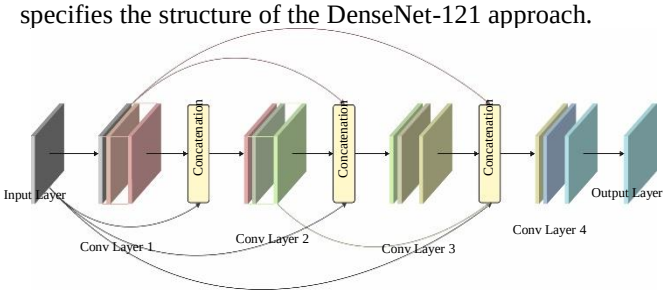

Fig. 3 DenseNet-121 framework

DenseNet-121 comprises 121 layers and is known for its dense connectivity technique; every layer links to every other layer in a feed-forward manner for the highest data flow among layers. The dense convolutional network (DenseNet) structure connects feature mapping, learned by different layers, rather than summing them as in conventional CNNs. This enhances data flow in the network, inspires feature reuse, mitigates redundancy, and optimises parameters.

DenseNets attain advanced accuracy with fewer parameters and calculations than ResNets. The DenseNet121 structure consists of four dense blocks with a growth rate (k) of 32. Before the main dense block, the model includes a 7×7 convolutional layer with 64 channels (stride 2), followed by a 3×3 max pooling layer.

The dense blocks attribute densely related convolutional layers, where every layer takes each prior feature map as input. In a dense block, layers contain ReLU activation, Batch Normalization (BN), a 1x1 convolution (a layer of bottleneck), and a 3x3 convolution.

Transition layers among dense blocks do convolution, operate BN, and integrate a 1x1 convolutional layer, which is followed by 2x2 average pooling with a compression factor (θ) of 0.5. The concluding dense block yields feature maps of fluctuating dimensions, which leads to global average pooling over a Fully Connected (FC) Softmax layer.

With 7 million parameters and $L(L+1)/2$ direct links within every dense block, DenseNet-121 is highly effective due to its advanced connectivity and excellent efficacy in numerous Computer Vision (CV) tasks. Its compact architecture enables deep supervision and alleviates vanishing gradients, making it appropriate for real-time and resource-constrained applications. Additionally, it promotes efficient feature propagation and reusability, enhancing learning efficiency.

3.3. LULC Classification: VAE

In addition, the VAE model is utilized for the LULC classification process [40]. This model is selected because it can learn latent representations while modelling data uncertainty. Unlike conventional classifiers, VAE integrates a probabilistic approach, allowing it to handle noisy and ambiguous data more effectively, a common scenario in RS. It compresses high-dimensional features into a lower-dimensional latent space, capturing the underlying structure of LULC patterns. This improves generalization and mitigates overfitting, particularly in scenarios with restricted labelled data. Compared to conventional AEs or deterministic classifiers, VAE presents improved robustness and adaptability to diverse land cover types. The model's generative behaviour also enables reconstruction-based anomaly detection, thereby improving classification reliability. Figure 4 illustrates the VAE structure.

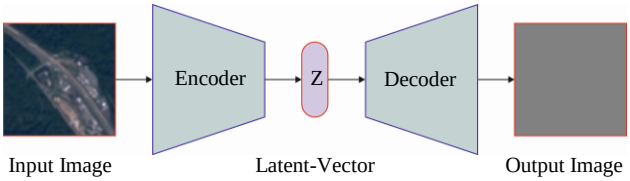

Fig. 4 VAE architecture

VAE is an excellent generative method. Although there are numerous models, VAE is used as it encrypts data into a probabilistic latent space, which enables a more refined perception of data distribution. It aids in taking into account the complexity and variability of standard functioning conditions, which makes it simpler to classify deviations. Compared to typical AEs and other techniques, VAEs ensure simplification by sampling from the discovered distribution of the latent space. VAEs efficiently reconstruct inputs by learning the underlying data distribution instead of memorizing cases. They compare original inputs with reconstructions from latent space, which helps highlight anomalies and is crucial in industries where normal operating conditions can vary. Due to this, the VAE technique is employed. The VAE structure comprises dual-core modules, including encoding and decoding. It is vital for the process and permits the method to acquire probabilistic input data symbols.

In VAE, the encoder maps input data A to a latent space by producing the parameters of a probability distribution, usually a Gaussian, defined by mean μ and variance. σ^2 instead of generating a single deterministic output. The mathematical formulation is stated in Equation (1) as

$$q(c_o|A) = \mathcal{N}\big(C; \mu(A), \sigma^2(A)\big) \quad (1)$$

Here, $q(c|A)$ denotes an approximate posterior distribution. The main objective of the encoder is to certify that this distribution thoroughly equals a previous distribution $p(c_o)$, which is frequently selected as a normal distribution $N(0, I)$

The decoding process reverses the operation by transforming latent space representations back into the data space. The decoding outputs for a distribution over the reconstructed data are shown as,

$$p(A|C) = \mathcal{N}\big(A; \mu'(C), \sigma'^2(C)\big) \quad (2)$$

While $\mu'(C)$ refers to the mean and $\sigma'^2(C)$ signifies the variance in the latent variable c. The objective of decoding is to exploit the probability of reconstructing the original data from the latent representation.

The VAE loss function integrates reconstruction error for accurate input recovery and KL divergence to regularize the latent space, enhancing generalization and meaningful output generation. The mathematical formulation is provided below,

$$Reconstruction\ Loss\ = \mathbb{E}_{q(C|A)}[\log p(A|C)] \quad (3)$$

While A signifies an original input, z denotes the latent variable, and $p(AC)$ emphasizes the probability of reconstructing x given c. Gaussian distribution is mainly employed for more constant data, which leads to a reconstruction loss calculated through MSE. The BCE is used for the dual data that is computed below.

$$BCE = -\frac{1}{N}\sum_{i=1}^{N}\big[A_i \log(A_i) + (1 - A_i)\log\big(1 - \hat{A}_i\big)\big] \quad (4)$$

The loss function ensures decoded outputs closely match the original inputs, enabling accurate reconstructions. KL divergence aligns the learned latent distribution with a prior distribution, promoting an organized latent space that supports generating diverse new samples. The mathematical formulation of the KL divergence is provided below,

$$D_{KL}(q(C|A)\|p(C)) = -\frac{1}{2}\sum_{j=1}^{d}\big(1 + \log\big(\sigma_j^2\big) - \mu_j^2 - \sigma_j^2\big) \quad (5)$$

Here, d is signified as dimensionality; σ_j and μ_j Represent the variance and mean of $the\ jth$ latent space, respectively.

3.4. Parameter Tuning: TSO Approach

Finally, the TSO method optimally adjusts the VAE model's hyperparameter values, leading to improved classification performance. This method is implemented for its robust search capabilities and adaptive exploration mechanisms. The model is motivated by the intellectual hunting characteristics of tuna fish. The model balances exploration and exploitation effectively, assisting in the avoidance of local minima —a common issue in optimization tasks. Unlike conventional models such as grid or random search, TSO dynamically adjusts parameters based on the search environment, resulting in faster convergence and improved outcomes. It is computationally efficient and scalable, making it appropriate for tuning intrinsic DL models. Moreover, its bio-inspired strategy gives flexibility and robustness across diverse datasets and problem settings. This makes TSO a highly effective tool for improving overall model performance in LULC classification tasks. Figure 5 specifies the flow of the TSO model.

The TSO technique depends on the foraging behaviour of the tuna swarms [41]. It employs two distinct foraging tactics, namely parabolic foraging and spiral foraging, to

create an effective meta-heuristic model. The mathematical process of the TSO model is given below:

Initialization. Like other meta-heuristic techniques that rely on swarm intelligence, the TSO optimizer procedure begins by randomly and uniformly creating initial populations in the search space.

$$Y_i^{int} = rand.(UB - LB) + LB \tag{6}$$

Here, Y_i^{int} Represents an initial individual at index i, UB and LB specify the upper and lower limits, respectively. Correspondingly, P denotes the population size of tuna, and $rand$ denotes a randomly generated vector value, which is evenly distributed between 0 and 1.

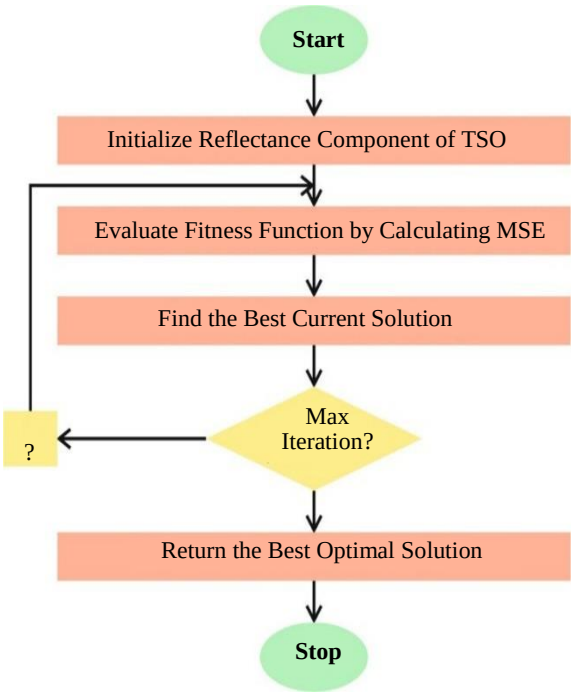

Fig. 5 Workflow of the TSO technique

3.4.1. Spiral Foraging

When they encounter predators, a group of small fish, such as sardines and herring, forms a dense, constantly shifting formation that makes it difficult for the predators to select a specific target.

However, tuna establish themselves in a tight spiral while chasing prey. While most fish lose direction, they jointly swim when a small set takes off from an assumed direction. Other fish modify their direction simultaneously to create a greater set with a similar hunting objective. To evade their predators, tuna schools broadcast data among themselves, allowing individual fish to follow one another.

$$Y_i^{t+1} = \begin{cases} \beta_1(Y_{best}^t + \alpha \cdot |Y_{best}^t - Y_i^t|) + \beta_2 \cdot Y_i^t \\ if\ i = 1 \\ \beta_1 \cdot (Y_{best}^t + \alpha \cdot |Y_{best}^t - Y_i^t|) + \beta_2 \cdot Y_{i-1}^t \\ if\ i = 1,2,\dots,P \end{cases} \tag{7}$$

$$\beta_1 = b + (1-b) \cdot \frac{I}{I_{\max}} \tag{8}$$

$$\beta_2 = (1-b) - (1-b) \cdot \frac{I}{I_{\max}} \tag{9}$$

$$\alpha = e^{ck} \cdot \cos(2\pi c) \tag{10}$$

$$k = e^3 \cdot cos\left(\left(\left(\frac{I_{\max}+1}{I}\right) - 1\right)\pi\right) \tag{11}$$

While Y_i^{r+1} depicts the ith individual in the subsequent iteration, Y_{best}^t represents the present best individual; β_1 and β_2 denote factors which influence how numerous individuals are drained near the optimum individual and their preceding location; b means a constant that defines how many individuals follow an optimum individual and their preceding location at the beginning; I denotes the present number of iterations. $I_{\max}$ depicts the maximal iteration count, and b denotes an arbitrary number between 0 and 1.

When a set of fish spins near the potential prey in a spiral form, it can efficiently hunt for food. However, if the most expert fish fail to discover food, it is impossible to feed as a group efficiently by following the foremost fish.

A reference point for the spiral hunt was generated as a random position in the search region, enabling every fish to explore a broader search space and facilitating the search for the entire group. The complete mathematical method is formed below:

$$Y_i^{(t+1)} = \begin{cases} \beta_1 \cdot Y_{rand}^t + \alpha \cdot |Y_{rand}^t - Y_i^t| + \beta_2 \cdot Y_i^t \\ if\ i = 1 \\ \beta_1 \cdot (Y_{rand}^t + \alpha \cdot |Y_{rand}^t - Y_i^t|) + \beta_2 \cdot Y_{(i-1)}^t \\ if\ i = 1,2,\dots,P \end{cases} \tag{12}$$

Here, a randomly produced reference point, Y_{rand}^tIt is recognized in the search space.

Meta-heuristic calculations are initiated with dispersion in space, gradually converging on more effective areas over time. Numerous locally best-fitting points serve as novel references in the spiral search; therefore, the TSO continues to move them while repeating near-better fitness processes. This eventually leads to the below-mentioned mathematical formulation that signifies the strategy of spiral foraging:

$$Y_i^{(r+1)} = \begin{cases} \beta_1 \cdot (Y_{rand}^t + \alpha \cdot |Y_{rand}^t - Y_i^t| + \beta_2 \cdot Y_i^t) \\ if\ rand < \dfrac{t}{t_{max}}, i = 1 \\ \beta_1 \cdot (Y_{rand}^t + \alpha \cdot |Y_{best}^t - Y_i^t| + \beta_2 \cdot Y_{(i-1)}^t) \\ if\ rand < \dfrac{t}{t_{max}}, i = 2,3, \dots, P \\ \beta_1 \cdot (Y_{best}^t + \rho \cdot |Y_{rand}^t - Y_i^t| + \beta_2 \cdot Y_i^t) \\ if\ rand \geq \dfrac{t}{t_{max}}, i = 1 \\ \beta_1 \cdot (Y_{rand}^t + \rho \cdot |Y_{best}^t - Y_i^t| + \beta_2 \cdot Y_{(i-1)}^t) \\ if\ rand \geq \dfrac{t}{t_{max}}, i = 2,3, \dots, P \end{cases} \quad (13)$$

3.4.2. Parabolic Foraging

Tuna usually searches for food utilizing dual models. One strategy involves creating a coil-shaped cluster to feed, while the other involves searching in an arc, utilizing food as a reference point. These dual hunting models emerge simultaneously, and each can be chosen independently. The following mathematical method expresses this behaviour:

$$Y_i^{(t+1)} = \begin{cases} Y_{best}^t + rand \cdot (Y_{best}^t - Y_i^t) + RN \cdot r^2 \cdot (Y_{best}^t - Y_i^t) \\ if\ rand < 0.5 \\ RN \cdot r^2 \cdot Y_i^t, if rand \geq 0.5 \end{cases} \quad (14)$$

$$e = \left(1 - \frac{I}{I_{\max}}\right)^{\left(\frac{I}{I_{\max}}\right)} \quad (15)$$

While RN is arbitrarily set to both 1 and -1.

Fitness selection plays a substantial role in the performance of the TSO technique. It computes candidate solutions through an encoded system within a defined hyperparameter range. The TSO model prioritizes accuracy as the main criterion for designing its fitness function. The mathematical formulation is computed as follows:

$$Fitness = \max(P) \quad (16)$$

$$P = \frac{TP}{TP + FP} \quad (17)$$

Here, TP and FP denote the true and false positive values, respectively.

4. Performance Validation

The experimental evaluation of the RSLULCC-DLTSO methodology is examined by utilizing the EuroSat dataset [42].

Table 1 illustrates the dataset comprising 5000 instances with 10 classes (AnnualCrop, Forest, Highway, Herbaceous Vegetation, Industrial, Pasture, Residential, Sea Lake, Permanent Crop, and River). Figure 6 specifies the sample images.

Table 1. Dataset specification

Class	Sample Numbers
C 1	500
C 2	500
C 3	500
C 4	500
C 5	500
C 6	500
C 7	500
C 8	500
C 9	500
C 10	500
Overall Samples	**5000**

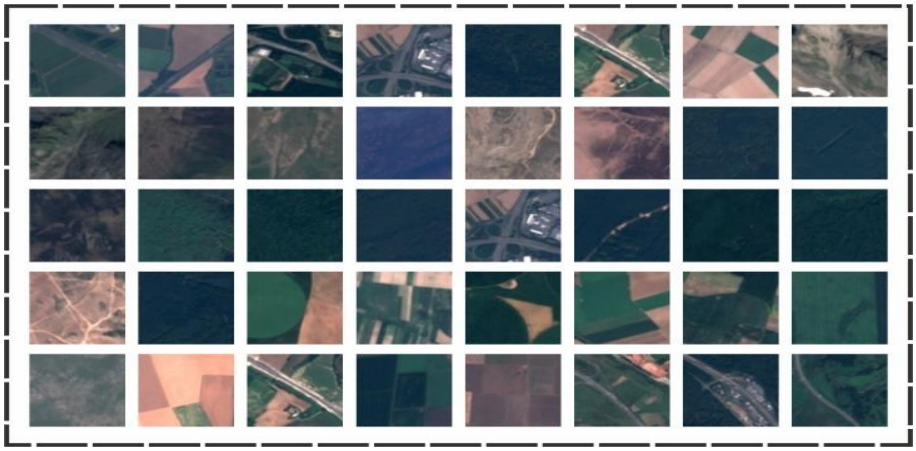

Fig. 6 Sample images

Figure 7 presents the classifier results of the RSLULCC-DLTSO methodology on the TR dataset. Figures 7(a)-7(b) present the confusion matrices, highlighting accurate classification across all 10 classes using 70% TRAPA and 30% TESPA. Figure 7(c)-7(d) illustrates high PR and ROC values, confirming effective performance for all class labels.

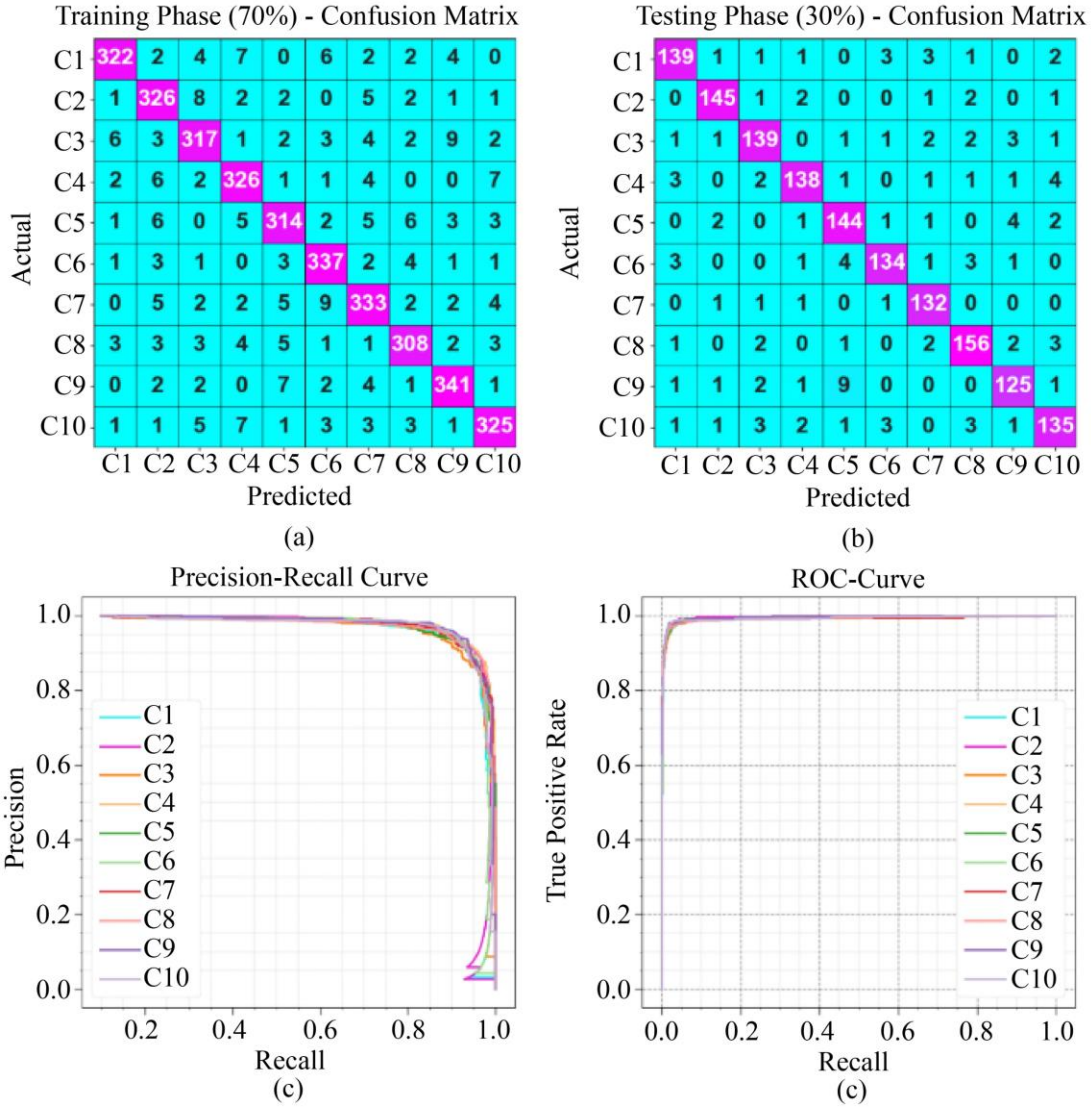

Fig. 7 (a-b) Confusion matrix, and (c-d) PR and ROC curves.

Table 2 and Figure 8 present the overall classification results of the RSLULCC-DLTSO approach for TRAPA values below 70% and TESPA values below 30%. The outcomes demonstrate that the RSLULCC-DLTSO approach accurately identified a variety of class labels. On 70% TRAPA, the RSLULCC-DLTSO technique provides an average $accu_y$, $prec_n$, $reca_l$, F_{score}, and $G_{measure}$ of 98.57%, 92.85%, 92.82%, 92.82%, and 92.83%, correspondingly. Besides, on 30% TESPA, the RSLULCC-DLTSO approach provides an average $accu_y$, $prec_n$, $reca_l$, F_{score}, and $G_{measure}$ of 98.49%, 92.48%, 92.47%, 92.46%, and 92.47%, respectively.

Table 2. Classification outcome of RSLULCC-DLTSO approach below 70%TRAPA and 30%TESPA

Classes	$Accu_y$	$Prec_n$	$Reca_l$	F_{Score}	$G_{Measure}$
TRAPA (70%)					
C1	98.80	95.55	92.26	93.88	93.89
C2	98.49	91.32	93.68	92.48	92.49
C3	98.31	92.15	90.83	91.49	91.49
C4	98.54	92.09	93.41	92.75	92.75
C5	98.37	92.35	91.01	91.68	91.68

C6	98.77	92.58	95.47	94.00	94.01
C7	98.26	91.74	91.48	91.61	91.61
C8	98.66	93.33	92.49	92.91	92.91
C9	98.80	93.68	94.72	94.20	94.20
C10	98.66	93.66	92.86	93.26	93.26
Average	**98.57**	**92.85**	**92.82**	**92.82**	**92.83**
TESPA (30%)					
C1	98.53	93.29	92.05	92.67	92.67
C2	99.07	95.39	95.39	95.39	95.39
C3	98.40	92.05	92.05	92.05	92.05
C4	98.53	93.88	91.39	92.62	92.63
C5	98.13	89.44	92.90	91.14	91.16
C6	98.53	93.71	91.16	92.41	92.42
C7	99.00	92.31	97.06	94.62	94.65
C8	98.47	92.86	93.41	93.13	93.13
C9	98.20	91.24	89.29	90.25	90.26
C10	98.07	90.60	90.00	90.30	90.30
Average	**98.49**	**92.48**	**92.47**	**92.46**	**92.47**

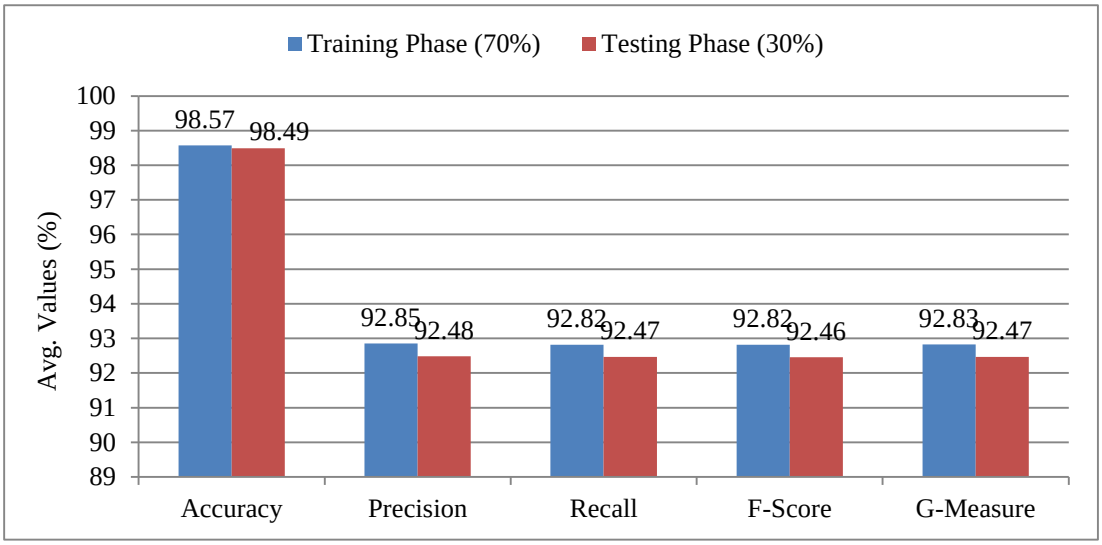

Fig. 8 Average of RSLULCC-DLTSO approach below 70%TRAPA and 30%TESPA

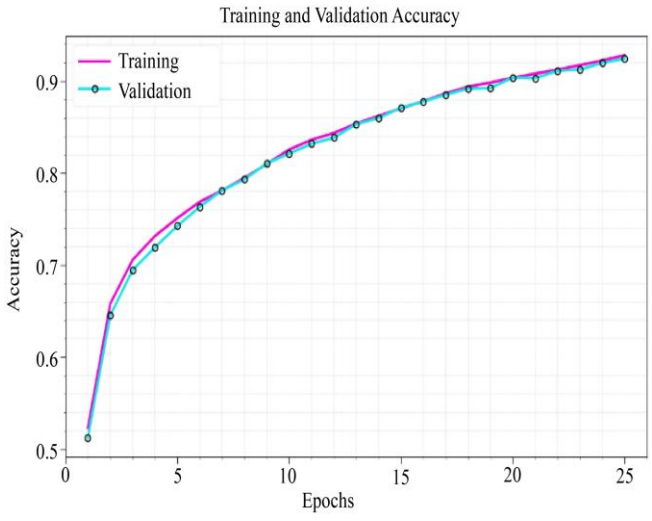

Fig. 9 $Accu_y$ analysis of the RSLULCC-DLTSO methodology

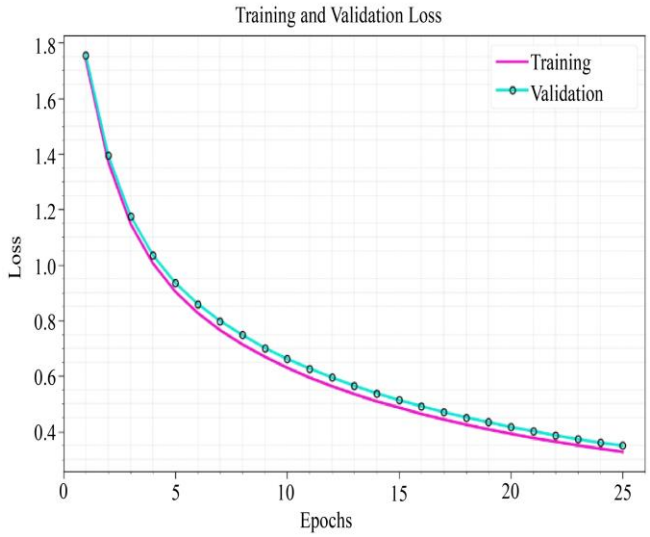

Fig. 10 Loss graph of the RSLULCC-DLTSO methodology

Figure 9 demonstrates the TRA $accu_y$ (TRAAY) and validation $accu_y$ (VLAAY) outcomes of the RSLULCC-DLTSO methodology over 0-25 epochs. The figure shows increasing trends for TRAAY and VLAAY, illustrating growth with more iterations. The consistent TRAAY and VLAAY values indicate mitigated overfitting and reliable predictions on unseen data. Figure 10 illustrates the TRA loss (TRALO) and VLA loss (VLALO) curves of the RSLULCC-DLTSO approach over 0-25 epochs. The decreasing TRALO and VLALO values indicate that the RSLULCC-DLTSO technique effectively balances data fitting and model simplification. This steady loss reduction confirms optimal tuning and enhanced prediction performance. To establish the proficiency of the RSLULCC-DLTSO approach, a thorough comparison analysis is illustrated in Table 3 and Figure 11 [43]. This solution indicates that the Shallow CNN method has performed poorly. Simultaneously, the GeoSystemNet, GoogleNet, and ResNet50 techniques have somewhat increased outcomes. Following the DenseNetl21, Inception V3, VGGl6, and LULCC-RFDADL approaches, these have established closer outcomes. Nevertheless, the RSLULCC-DLTSO method outperforms the other approaches with an increased $accu_y$ of 98.57%, $prec_n$ of 92.85%, $reca_l$ of 92.82%, and F_{score} of 92.82%.

Table 3. Comparison analysis of the RSLULCC-DLTSO methodology with existing methods [43]

Model	$Accu_y$	$Prec_n$	$Reca_l$	F_{Score}
Shallow CNN	87.99	85.43	81.68	84.43
GoogleNet	96.04	85.93	68.80	80.43
DenseNetl21	96.68	71.14	55.24	77.75
Inception V3	96.89	86.84	75.00	81.96
ResNet50	96.46	82.91	56.88	82.97
VGGl6	96.69	83.63	60.30	82.46
GeoSystemNet	94.69	89.35	68.30	88.41
LULCC-RFDADL	98.18	90.83	90.83	90.79
RSLULCC-DLTSO	98.57	92.85	92.82	92.82

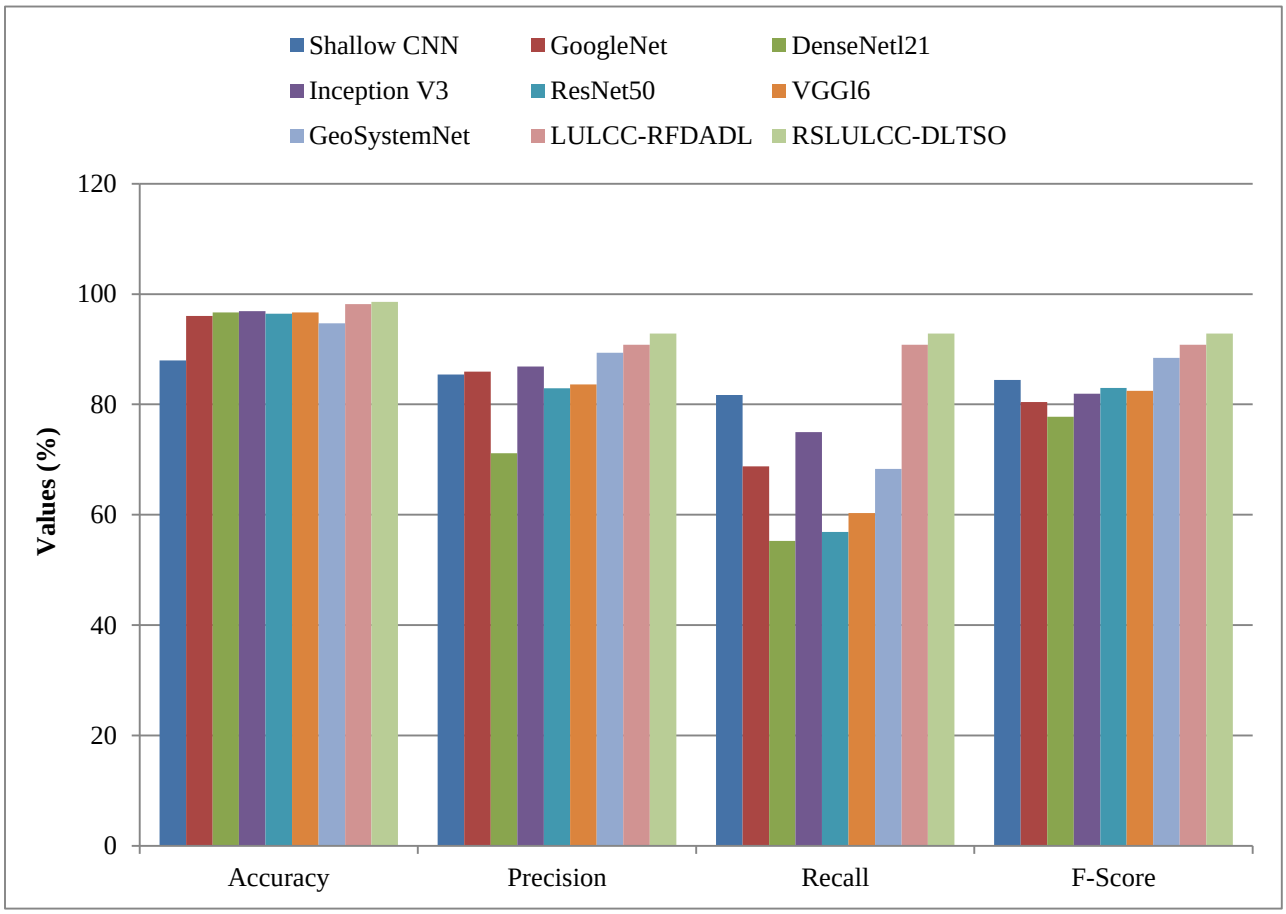

Fig. 11 Comparison analysis of the RSLULCC-DLTSO methodology with existing methods

Table 4. COMT outcome of the RSLULCC-DLTSO method with existing techniques

Model	COMT (sec)
Shallow CNN	2.10
Google Net	3.23
DenseNet-l21	3.16
Inception-V3	2.22
ResNet-50	2.07
VGG-l6	2.26
GeoSystemNet	2.24
LULCC-RFDADL	0.97
RSLULCC-DLTSO	0.41

The Computation Time (COMT) outcomes of the RSLULCC-DLTSO methodology are compared with those of other models in Table 4 and Figure 12. The solutions indicate that the RSLULCC-DLTSO technique achieves a COMT of 0.97s.

On the other hand, the Shallow CNN, DenseNet-l21, Google Net, InceptionV3, ResNet-50, VGG-l6, and GeoSystemNet techniques attain increased COMT values of 2.10s, 3.23s, 3.16s, 2.22s, 2.07s, 2.26s, 2.24s, and 0.97s, respectively. Thus, the RSLULCC-DLTSO methodology is used to classify LULC.

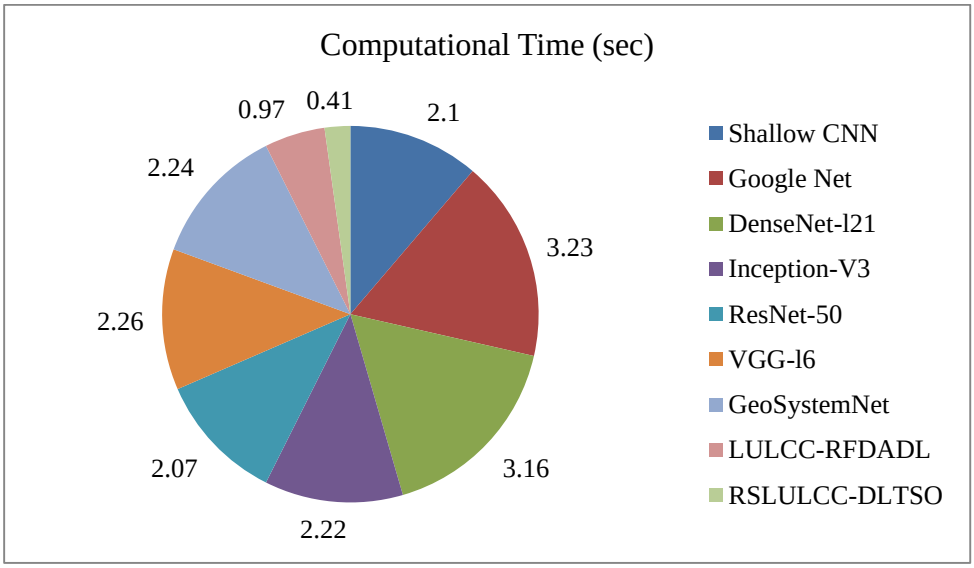

Fig. 12 COMT outcome of RSLULCC-DLTSO method with existing techniques

5. Conclusion

In this paper, a novel RSLULCC-DLTSO technique is proposed. The RSLULCC-DLTSO technique aims to advance intelligent and automated LULC classification systems that assist in sustainable land management and environmental decision-making. In the pre-processing stage, the RSLULCC-DLTSO technique utilizes WF to remove noise and enhance the quality of satellite images. Furthermore, the DenseNet-121-based feature extraction captures hierarchical spatial patterns and textures from RSI. In addition, the VAE model is utilized for LULC classification. Finally, the TSO model optimally tunes the hyperparameters of the VAE technique, resulting in improved classification. A wide range of simulation analyses of the RSLULCC-DLTSO approach is implemented under the EuroSat dataset. The comparative study of the RSLULCC-DLTSO approach illustrated a superior accuracy value of 98.57% compared to existing models.

References

[1] H.N. Mahendra, and S. Mallikarjunaswamy, "An Analysis of Change Detection in Land Use Land Cover Area of Remotely Sensed Data using Supervised Classifier," *International Journal of Environmental Technology and Management*, vol. 26, no. 6, pp. 498-511, 2023. [CrossRef] [Google Scholar] [Publisher Link]

[2] Kavita Bhosle, and Vijaya Musande, "Evaluation of Deep Learning CNN Model for Land Use Land Cover Classification and Crop Identification using Hyperspectral Remote Sensing Images," *Journal of the Indian Society of Remote Sensing*, vol. 47, pp. 1949-1958, 2019. [CrossRef] [Google Scholar] [Publisher Link]

[3] Quoc Bao Pham et al., "Multi-Spectral Remote Sensing and GIS-based Analysis for Decadal Land Use Land Cover Changes and Future Prediction using Random Forest Tree and Artificial Neural Network," *Advances in Space Research*, vol. 74, no. 1, pp. 17-47, 2024. [CrossRef] [Google Scholar] [Publisher Link]

[4] Carolina Acuña-Alonso et al., "Development of a Convolutional Neural Network to Accurately Detect Land Use and Land Cover," *MethodsX*, vol. 12, pp. 1-9, 2024. [CrossRef] [Google Scholar] [Publisher Link]

[5] Yinghui Zhao et al., "Spatio-Temporal Land-Use/LandCover Change Dynamics in Coastal Plains in Hangzhou Bay Area, China from 2009 to 2020 Using Google Earth Engine," *Land*, vol. 10, no. 11, pp. 1-31, 2021. [CrossRef] [Google Scholar] [Publisher Link]

[6] Sekela Twisa et al., "Evaluating and Predicting the Effects of Land Use Changes on Hydrology in Wami River Basin, Tanzania," *Hydrology*, vol. 7, no. 1, pp. 1-18, 2020. [CrossRef] [Google Scholar] [Publisher Link]

[7] Shahzaib Ashraf, and Saleem Abdullah, "Decision Support Modeling for Agriculture Land Selection based on Sine Trigonometric Single Valued Neutrosophic Information," *International Journal of Neutrosophic Science*, vol. 9, no. 2, pp. 60-73, 2020. [CrossRef] [Google Scholar] [Publisher Link]

[8] B. Liu, S. Du, and X. Zhang, "Land Cover Classification Using Convolutional Neural Network with Remote Sensing Data and Digital Surface Model," *ISPRS Annals of the Photogrammetry, Remote Sensing and Spatial Information Sciences*, vol. 3, pp. 39-43, 2020. [CrossRef] [Google Scholar] [Publisher Link]

[9] Manuel Carranza-García, Jorge García-Gutiérrez, and José C. Riquelme, "A Framework for Evaluating Land Use and Land Cover Classification using Convolutional Neural Networks," *Remote Sensing*, vol. 11, no. 3, pp. 1-23, 2019. [CrossRef] [Google Scholar] [Publisher Link]

[10] Supattra Puttinaovarat, Kanit Khaimook, and Paramate Horkaew, "Land Use and Land Cover Classification from Satellite Images based on Ensemble Machine Learning and Crowdsourcing Data Verification," *International Journal of Cartography*, vol. 11, no. 1, pp. 3-23, 2025. [CrossRef] [Google Scholar] [Publisher Link]

[11] Leo Thomas Ramos, and Angel D. Sappa, "Leveraging U-Net and Selective Feature Extraction for Land Cover Classification using Remote Sensing Imagery," *Scientific Reports*, vol. 15, pp. 1-17, 2025. [CrossRef] [Google Scholar] [Publisher Link]

[12] Saddaf Rubab et al., "A Novel Network Level Fusion Architecture of Proposed Self-Attention and Vision Transformer Models for Land Use and Land Cover Classification from Remote Sensing Images," *IEEE Journal of Selected Topics in Applied Earth Observations and Remote Sensing*, vol. 17, pp. 13135-13148, 2024. [CrossRef] [Google Scholar] [Publisher Link]

[13] Soheil Majidi, Ghazale Babapour, and Reza Shah-Hosseini, "An Encoder–Decoder Network for Land Cover Classification using a Fusion of Aerial Images and Photogrammetric Point Clouds," *Survey Review*, vol. 57, no. 400, pp. 55-64, 2025. [CrossRef] [Google Scholar] [Publisher Link]

[14] Madhusmita Sahu, and Rasmita Dash, "Cognitive Land Cover Mapping: A Three-Layer Deep Learning Architecture for Remote Sensing Data Classification," *Environmental Challenges*, vol. 15, pp. 1-13, 2024. [CrossRef] [Google Scholar] [Publisher Link]

[15] Yang Tang et al., "Weakly Supervised Land-Cover Classification of High-Resolution Images with Low-Resolution Labels through Optimized Label Refinement," *International Journal of Remote Sensing*, vol. 46, no. 5, pp. 1913-1937, 2025. [CrossRef] [Google Scholar] [Publisher Link]

[16] P. Adlene Ebenezer, and S. Manohar, "Land Use/Land Cover Change Classification and Prediction Using Deep Learning Approaches," *Signal, Image and Video Processing*, vol. 18, pp. 223-232, 2024. [CrossRef] [Google Scholar] [Publisher Link]

[17] Junqing Huang et al., "LCCDMamba: Visual State Space Model for Land Cover Change Detection of VHR Remote Sensing Images," *IEEE Journal of Selected Topics in Applied Earth Observations and Remote Sensing*, vol. 18, pp. 5765-5781, 2025. [CrossRef] [Google Scholar] [Publisher Link]

[18] L. Gowri et al., "Remote Sensing Based Land Cover Classification Using Residual Feature—Hyper Graph Convolutional Neural Network (HGCNN)," *Journal of the Indian Society of Remote Sensing*, vol. 53, pp. 2105-21220, 2025. [CrossRef] [Google Scholar] [Publisher Link]

[19] Saeed Alqadhi et al., "Applying Deep Learning to Manage Urban Ecosystems in Arid Abha, Saudi Arabia: Remote Sensing-Based Modelling for Ecological Condition Assessment and Decision-Making," *Heliyon*, vol. 10, no. 4, pp. 1-20, 2024. [CrossRef] [Google Scholar] [Publisher Link]

[20] Muhammad Kashif Bhatti et al., "A Novel Approach for High-Resolution Coastal Areas and Land Use Recognition from Remote Sensing Images based on Multimodal Network-Level Fusion of SRAN3 and Lightweight Four Encoders ViT," *IEEE Journal of Selected Topics in Applied Earth Observations and Remote Sensing*, vol. 18, pp. 6844-6858, 2025. [CrossRef] [Google Scholar] [Publisher Link]

[21] M. Rega, and S. Sivakumar, "Enhancing Remote Sensing Image Classification using Horse Herd Optimization with Deep Transfer Learning Model," *2024 International Conference on Cognitive Robotics and Intelligent Systems (ICC - ROBINS)*, Coimbatore, India, pp. 200-205, 2024. [CrossRef] [Google Scholar] [Publisher Link]

[22] Rohan Vaghela et al., "Land Cover Classification for Identifying the Agriculture Fields Using Versions of YOLO V8," *IEEE Journal of Selected Topics in Applied Earth Observations and Remote Sensing*, vol. 18, pp. 8672-8684, 2025. [CrossRef] [Google Scholar] [Publisher Link]

[23] Sackdavong Mangkhaseum et al., "Flood Susceptibility Mapping Using Publicly Available Big Data with Google Earth Engine and Deep Learning Algorithms," *2024 5th International Conference on Big Data Analytics and Practices (IBDAP)*, Bangkok, Thailand, pp. 38-43, 2024. [CrossRef] [Google Scholar] [Publisher Link]

[24] J. Jayanth et al., *Chapter 11 - Detecting the Stages of Ragi Crop Diseases using Satellite Data in Villages of Nanjangud Taluk*, Hyperautomation in Precision Agriculture, Academic Press, pp. 131-145, 2025. [CrossRef] [Google Scholar] [Publisher Link]

[25] Junfu Fan et al., "DDPM-SegFormer: Highly Refined Feature Land Use and Land Cover Segmentation with a Fused Denoising Diffusion Probabilistic Model and Transformer," *International Journal of Applied Earth Observation and Geoinformation*, vol. 133, pp. 1-16, 2024. [CrossRef] [Google Scholar] [Publisher Link]

[26] Alex Okiemute Onojeghuo, Christopher E. Ndehedehe, and Ajoke Ruth Onojeghuo, "Deep Learning-Assisted Mapping of Wetland Dynamics in the Niger Delta Using Open-Access Multi-Sensor Remote Sensing Data," *Environmental and Earth Sciences*, pp. 1-34, 2025. [CrossRef] [Google Scholar] [Publisher Link]

[27] Jian Lu et al., "GOA-Optimized Deep Learning for Soybean Yield Estimation using Multi-Source Remote Sensing Data," *Scientific Reports*, vol. 14, pp. 1-19, 2024. [CrossRef] [Google Scholar] [Publisher Link]

[28] P. Shailaja et al., "LCC-Net: Swin Transformer-CNN Hybrid for Enhanced Land Cover Classification in Natural Disaster Monitoring," *Systems and Soft Computing*, vol. 7, pp. 1-14, 2025. [CrossRef] [Google Scholar] [Publisher Link]

[29] Suraj Sawant, and Jayanta Kumar Ghosh, "Land Use Land Cover Classification using Sentinel Imagery Based on Deep Learning Models," *Journal of Earth System Science*, vol. 133, pp. 1-23, 2024. [CrossRef] [Google Scholar] [Publisher Link]

[30] Mashael Maashi et al., "Forecasting Land Use Changes in Crop Classification and Drought Using Remote Sensing," *Journal of Arid Land*, vol. 17, pp. 575-589, 2025. [CrossRef] [Google Scholar] [Publisher Link]

[31] Athanasia Chroni et al., "Fusing Multispectral and LiDAR Data for CNN-Based Semantic Segmentation in Semi-Arid Mediterranean Environments: Land Cover Classification and Analysis," *Remote Sensing*, vol. 16, no. 15, pp. 1-30, 2024. [CrossRef] [Google Scholar] [Publisher Link]

[32] Girmaw Abebe Tadesse et al., "Enhancing Food Security with High-Quality Land-Use and Land-Cover Maps: A Local Model Approach," *IEEE Journal of Selected Topics in Applied Earth Observations and Remote Sensing*, vol. 18, pp. 15265-15277, 2025. [CrossRef] [Google Scholar] [Publisher Link]

[33] Romie Jhonnerie et al., "Integration of Generative Artificial Intelligence and Google Earth Engine for Mangrove Land Cover Mapping," *BIO Web of Conferences*, vol. 136, pp. 1-17, 2024. [CrossRef] [Google Scholar] [Publisher Link]

[34] Quang-Hieu Tang et al., "A Deep-Learning Framework for Land-Sliding Classification from Remote Sensing Image," *arXiv preprint*, pp. 1-11, 2025. [CrossRef] [Google Scholar] [Publisher Link]

[35] Won-Kyung Baek, Moung-Jin Lee, and Hyung-Sup Jung, "Land Cover Classification from RGB and NIR Satellite Images using Modified U-Net Model," *IEEE Access*, vol. 12, pp. 69445-69455, 2024. [CrossRef] [Google Scholar] [Publisher Link]

[36] Alelgn Ewunetu, and Gebeyehu Abebe, "Integrating Google Earth Engine and Random Forest for Land Use and Land Cover Change Detection and Analysis in the Upper Tekeze Basin," *Earth Science Informatics*, vol. 18, pp. 1-16, 2025. [CrossRef] [Google Scholar] [Publisher Link]

[37] Bilal Arain et al., "Deep Learning Framework for Land Cover and Land Use Classification: Five Case Studies with Hyperspectral and RGB Imagery," *SSRN*, pp. 1-56, 2024. [CrossRef] [Google Scholar] [Publisher Link]

[38] Manas Ranjan Prusty, Rohit Madhavan Sudharsan, and Philip Anand, "Enhancing Medical Image Classification with Generative AI using Latent Denoising Diffusion Probabilistic Model and Wiener Filtering Approach," *Applied Soft Computing*, vol. 161, 2024. [CrossRef] [Google Scholar] [Publisher Link]

[39] Farid et al., "Bangladeshi Vehicle Classification and Detection using Deep Convolutional Neural Networks with Transfer Learning," *IEEE Access*, vol. 13, pp. 26429-26455, 2025. [CrossRef] [Google Scholar] [Publisher Link]

[40] Praveen Vijai, and Bagavathi Sivakumar, "Anomaly Detection Solutions: The Dynamic loss Approach in VAE for Manufacturing and IoT Environment," *Results in Engineering*, vol. 25, pp. 1-14, 2025. [CrossRef] [Google Scholar] [Publisher Link]

[41] Mohamad Khayat et al., "Blockchain-Powered Secure and Scalable Threat Intelligence System with Graph Convolutional Autoencoder and Reinforcement Learning Feedback Loop," *IEEE Access*, vol. 13, pp. 24736-24748, 2025. [CrossRef] [Google Scholar] [Publisher Link]

[42] EuroSat Dataset, Kaggle, [Online]. Available: https://www.kaggle.com/datasets/apollo2506/eurosat-dataset

[43] Mohammed Aljebreen et al., "Land Use and Land Cover Classification Using River Formation Dynamics Algorithm with Deep Learning on Remote Sensing Images," *IEEE Access*, vol. 12, pp. 11147-11156, 2024. [CrossRef] [Google Scholar] [Publisher Link]